Homogeneous Amorphization in High-Energy Ion Implanted Si

T. Motooka, S. Harada, and M. Ishimaru

Department of Materials Science and Engineering, Kyushu University, Fukuoka 812, Japan

(Received 9 July 1996)

We have investigated amorphization mechanisms in 5 MeV Si^+ ion implanted Si using cross-sectional transmission electron microscopy (XTEM) measurements. Both microdiffraction patterns and high-resolution XTEM images of the amorphous/crystalline (*a*/*c*) Si interface region indicate that the *a*/*c* interface is very sharp and the amorphous Si transition occurs within a few atomic layers. Image simulations based on the divacancy and di-interstitial (*D*-*D*) pair model [Phys. Rev. B **49**, 16 367 (1994)] suggest that an accumulation of the *D*-*D* pairs gives rise to homogeneous amorphization in ion implanted Si. [S0031-9007(97)02961-X]

PACS numbers: 61.16.–d, 61.50.Ks, 61.72.–y, 61.80.Jh

Ion implantation is an important technique for precise impurity doping in Si microelectronics devices. As device sizes are decreased, it is increasingly important to understand atomistic pictures of the structural transformation in Si during ion implantation. Although it is generally considered that ion-beam-induced damages give rise to amorphization, there are still controversial pictures on the amorphization mechanisms. More than 20 years ago, Morehead and Crowder [1] proposed their classic phenomenological model in which amorphization initially occurs in the cylindrical region around each ion path and the radius of this amorphized cylinder is determined by the rate of the outdiffusion of primary defects from the core region. Thus, in the Morehead and Crowder model, continuous amorphization of ion implanted Si is due to sufficient overlap of the amorphized cylindrical cascades and this amorphization mechanism is called heterogeneous amorphization. On the other hand, in the homogeneous amorphization model proposed initially by Swanson *et al.* [2] and recently by Holland *et al.* [3], amorphization is a phase transition induced by an accumulation of a sufficient number of defects in crystalline Si. More recently, one of us [4] has proposed, based on molecular dynamics (MD) calculations, a homogeneous amorphization model in which an accumulation of divacancy and di-interstitial (*D*-*D*) pairs gives rise to amorphization.

In this Letter, we have further investigated the amorphization mechanism of ion implanted Si by using high-resolution cross-sectional transmission electron microscopy (XTEM). Detailed analysis of the amorphous/crystalline (*a*/*c*) Si interface regions has been carried out by preparing high-energy self-ion implanted Si samples where amorphization can be observed throughout the region with a thickness of $\sim 2\ \mu$m. Observed lattice images have been compared with the results of image simulations for the damaged crystalline Si including various number of the *D*-*D* pairs.

Si^+ ion implantations were performed at room temperature in optically flat Czochralsky-grown *p*-type Si(100) substrates with a resistivity of 6–8 Ω cm. The substrates were oriented 5° off-normal to the incident ion beam for suppression of channeling effects. The ion energy was 5 MeV and the doses were 1×10^{17} and 2×10^{17} cm^{-2}. The ion current was set at 0.2 $\mu A/cm^2$ to avoid beam heating. XTEM observation was carried out using a 200 kV JEOL JEM-2000EX microscope for high-resolution images and JEM-2000FX for microdiffraction measurements, and these samples were prepared by a combination of mechanical polishing and ion milling with 3 keV Ar^+ ions. Image simulations were carried out by the multislice method [5] using an electron microscopy image simulation package [6].

Figures 1(a) and 1(b) show the XTEM dark-field images of the samples with doses of 1×10^{17} and 2×10^{17} cm^{-2}, respectively. Figure 1(c) shows the depth distribution of vacancies initially generated by 5 MeV Si^+ ion bombardment obtained by Monte Carlo simulations using TRIM [7]. The calculations were carried out for 10 000 ion histories in a full cascade mode assuming the Si threshold displacement energy of 13 eV and the lattice binding energy of 4.5 eV. Since the change in the vacancy concentration

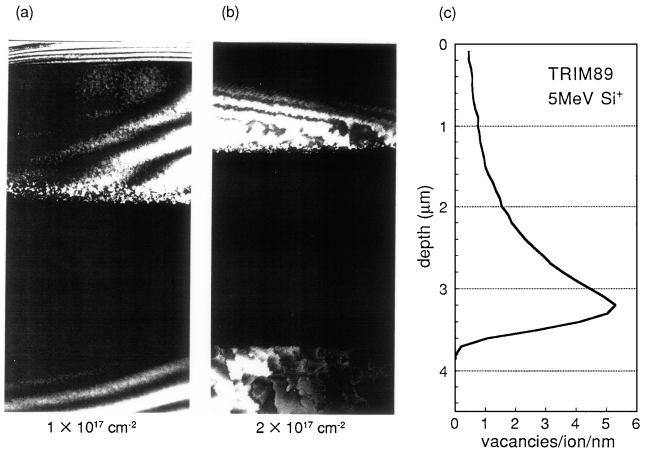

FIG. 1. Dark-field images of the samples with ion doses of (a) 1×10^{17} and (b) 2×10^{17} cm^{-2} as well as (c) the depth distribution of vacancies calculated by TRIM.

 0031-9007/97/78(15)/2980(3)$10.00

is much slower in the front part of the damaged region than in the *end of range* located around ~ 3.5 μm in depth, it is possible to estimate the critical vacancy concentration for amorphization by comparing the *a*/*c* interface observed in the depth of $1 \sim 2$ μm with the calculated depth distribution of vacancies. The obtained threshold vacancy concentration for amorphization is $\approx 2 \times 10^{24}$ cm^{-3}, which corresponds to $\approx$40 displacements per target atom (DPA) and is much larger than the typical threshold DPA, $\sim$1 for amorphization of Si observed in lower energy (100 keV) Si^+ ion implanted samples [8]. A similar *a*/*c* interface was obtained by 1.25 MeV, 10^{16} cm^{-2} Si^+ ion implantation at room temperature [9] where the threshold DPA was $\approx$10. These results suggest that the point defects concentration N generated during ion bombardments can be described by the rate equation $dN/dt = N_g - \alpha N$. Here N_g is the primary point-defects generation rate corresponding to the DPA and αN (α: a constant) the annealing rate due to the electronic excitation induced by fast moving ions. Assuming electronic annealing processes are much faster than thermal ones, the stationary point-defects concentration becomes N_g/α before the thermal recombination and clustering processes occur, and the observed threshold DPA $\approx$1 (100 keV), $\approx$10 (1.25 MeV), and $\approx$40 (5 MeV) can be obtained if α is proportional to (the electronic stopping power) $\times$ (excitation length per unit time) or v^2 (v: ion velocity).

Figure 2(a) shows the detailed bright-field image near the *a*/*c* interface of the sample with a dose of 1×10^{17} cm^{-2}. Diffraction patterns from the three selected areas with a size of $\sim$30 nm in diameter are also shown in Fig. 2(b). These diffraction patterns indicate that the *a*/*c* interface is very sharp and the diffraction spots corresponding to the (110) reciprocal-lattice plane of crystalline Si clearly appear even in the adjacent area to the completely amorphized region judged by the halo diffraction pattern. The results suggest that amorphization occurs homogeneously when the defect density exceeds the threshold value. Below the threshold defect density, an accumulation of defects seems to result in defected crystal including extending defects such as dislocation loops, as can be seen in Fig. 2(a).

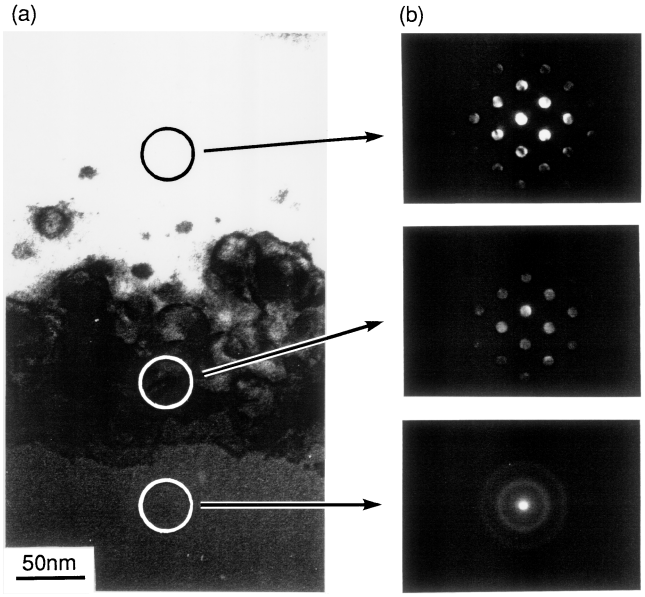

FIG. 2. (a) Bright-field image of the *a*/*c* interface region in the 1×10^{17} cm^{-2} sample. (b) Diffraction patterns from the selected areas indicated by the circles.

Figure 3 shows the high-resolution XTEM images taken in the $\langle 110 \rangle$ projection from the same sample described in Fig. 2. Near the surface region where the ion-beam-induced damage is relatively weak, the observed image [Fig. 3(a)] reveals almost the perfect crystalline Si contrast. On the other hand, in the *a*/*c* interface region [Fig. 3(b)], the crystalline image becomes deteriorated toward the amorphous region. Nevertheless, it should be noted that the crystalline image remains until the amorphous transition occurs within a few atomic layers which is consistent with the results obtained by the microdiffraction pattern described above. These results also suggest that homogeneous amorphization occurs in the present samples. It should be noted, however, that no sharp *a*/*c* interface was observed, and heterogeneous amorphization occurred in 1.25 MeV Si^+ ion implanted Si at liquid N_2 temperature [9].

We carried out image simulations of damaged Si based on our *D-D* pair model for amorphization processes during ion implantation in crystalline Si [4]. Figure 4 shows the calculated radial distribution functions (RDF) and simulated images of the Si lattices with the *D-D* pair concentrations per atom $c = 0.1, 0.2, 0.3, 0.4$, and 0.5 together with the high-resolution images from the areas A, B, C, D, and E as indicated in Fig. 3. Various numbers of the *D-D* pairs corresponding to these *c* values were first introduced in the diamond cubic cluster composed of 512 Si atoms with periodic boundary conditions. Then Langevin

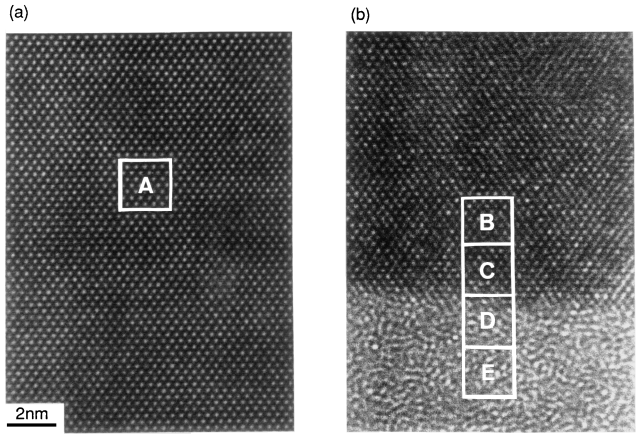

FIG. 3. High-resolution images of the 1×10^{17} cm^{-2} sample: (a) Near the surface and (b) the *a*/*c* interface. Selected areas marked by A, B, C, D, and E are compared with the results of image simulations shown in Fig. 4.

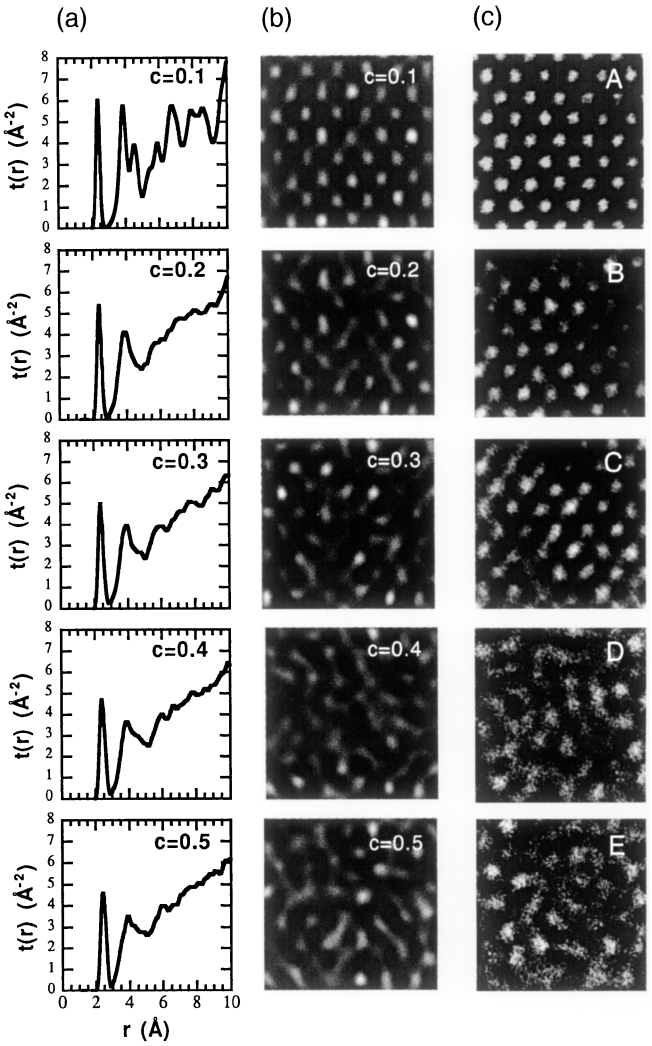

FIG. 4. Calculated radial distribution functions (a) and lattice images (b) of damaged Si with various *D-D* pair concentrations together with the high-resolution images (c) from the areas A, B, C, D, and E in Fig. 3. Image simulation conditions are aperture size = 10 nm^{-1}, spherical aberration coefficient = 1.2 mm, defocus value = −90 nm, and sample thickness = 9 nm.

MD simulations were performed at 0 K to determine the stable atomic configurations using the Tersoff empirical potential [10] with a time step of 0.001 ps and a friction constant of $\gamma = 15/\text{ps}$ [11]. For the multislice image calculations, the aperture size, spherical aberration coefficient, and defocus value were set to follow the experimental ones 10 nm^{-1}, 1.2 mm, and −90 nm, respectively, while the sample thickness was adjusted to be 9 nm where the crystalline Si-like image was well reproduced.

At $c = 0.1$, higher order peaks corresponding to more than the second nearest neighbor still remain in RDF and the lattice image is crystal-like similar to that from the area A [see Fig. 3(a)]. Although the RDF for $c = 0.2$ resembles that of *a*-Si observed experimentally [12], the corresponding lattice image still indicates some crystalline order. This is, as was suggested by Wooten and Weaire [13], due to the large distortion of bond angles which results in a dramatic change in the RDF. The crystalline order is substantially destroyed at $c = 0.3$, however, and the simulated images for $c = 0.4$ and 0.5 are in good agreement with the observed ones obtained from the completely amorphized areas indicated by D and E [see Fig. 3(b)]. Comparing the observed change in the lattice images B to E around the *a*/*c* interface region with that in the simulated images $c = 0.2$ to 0.5, it is suggested that homogeneous amorphization is induced when the *D-D* pair concentration *c* exceeds ≈0.3.

In conclusion, we have shown strong evidence in support of a homogeneous amorphization mechanism in ion implanted Si and have identified a possible atomistic mechanism. Amorphization can be induced when the concentration of the *D-D* pairs exceeds the threshold value during ion implantation, while defected crystal is formed when the concentration is below the threshold value.

We would like to thank O. W. Holland and T. E. Hayens at Oak Ridge National Laboratory for providing high-energy ion implanted Si samples. This work was partly supported by the New Energy and Industrial Technology Development Organization through the Japan Space Utilization Promotion Center.

[1] F. F. Morehead, Jr. and B. L. Crowder, Radiat. Eff. **6**, 27 (1970).
[2] M. L. Swanson, J. R. Parsons, and C. W. Hoelke, Radiat. Eff. **9**, 249 (1971).
[3] O. W. Holland, S. J. Pennycook, and G. L. Albert, Appl. Phys. Lett. **55**, 2503 (1989).
[4] T. Motooka, Phys. Rev. B **49**, 16 367 (1994).
[5] J. M. Cowley and A. F. Moodie, Acta Crystallogr. **10**, 609 (1957).
[6] P. A. Stadelmann, Ultramicroscopy **21**, 131 (1987).
[7] J. P. Biersack, Nucl. Instrum. Methods **174**, 257 (1980).
[8] T. Motooka, F. Kobayashi, Y. Hiroyama, and T. Tokuyama, Jpn. J. Appl. Phys. **32**, 318 (1993).
[9] M. K. El-Ghor, O. W. Holland, C. W. White, and S. J. Pennycook, J. Mater. Res. **5**, 352 (1990).
[10] J. Tersoff, Phys. Rev. B **37**, 6991 (1988).
[11] T. Motooka, Y. Hiroyama, R. Suzuki, T. Ohdaira, Y. Hirano, and F. Sato, Nucl. Instrum. Methods Phys. Res., Sect. B **106**, 198 (1995).
[12] S. Kugler, G. Molnár, G. Petö, E. Zsoldos, L. Rosta, A. Menelle, and R. Bellissent, Phys. Rev. B **40**, 8030 (1989).
[13] F. Wooten and D. Weaire, *Solid State Physics* (Academic, New York, 1987), Vol. 40, p. 1.